NANO LETTERS

Letter

pubs.acs.org/NanoLett

Self-Propelling Nanomotors in the Presence of Strong Brownian Forces

Tung-Chun Lee,[†] Mariana Alarcón-Correa,[†,‡] Cornelia Miksch,[†] Kersten Hahn,[†] John G. Gibbs,[†] and Peer Fischer*[,†,‡]

[†]Max Planck Institute for Intelligent Systems, Heisenbergstrasse 3, 70569 Stuttgart, Germany

[‡]Inst. for Phys. Chem., Univ. Stuttgart, Pfaffenwaldring 55, 70569 Stuttgart, Germany

Supporting Information

ABSTRACT: Motility in living systems is due to an array of complex molecular nanomotors that are essential for the function and survival of cells. These protein nanomotors operate not only despite of but also because of stochastic forces. Artificial means of realizing motility rely on local concentration or temperature gradients that are established across a particle, resulting in slip velocities at the particle surface and thus motion of the particle relative to the fluid. However, it remains unclear if these artificial motors can function at the smallest of scales, where Brownian motion dominates and no actively propelled living organisms can be found. Recently, the first reports have appeared suggesting that the swimming mechanisms of artificial structures may also apply to enzymes that are catalytically active. Here we report a scheme to realize artificial Janus nanoparticles (JNPs) with an overall size that is comparable to that of some enzymes ∼30 nm. Our JNPs can catalyze the decomposition of hydrogen peroxide to water and oxygen and thus actively move by self-electrophoresis. Geometric anisotropy of the Pt−Au Janus nanoparticles permits the simultaneous observation of their translational and rotational motion by dynamic light scattering. While their dynamics is strongly influenced by Brownian rotation, the artificial Janus nanomotors show bursts of linear ballistic motion resulting in enhanced diffusion.

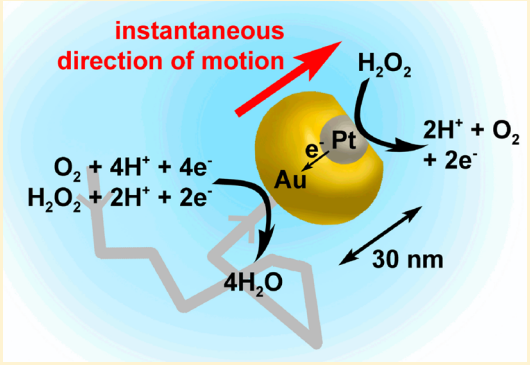

KEYWORDS: *Nanomotors, Janus particles, nanofabrication, dynamic light scattering, enhanced diffusion, self-propulsion*

Self-propelling motors and swimmers[1−13] serve as model systems for motile biological organisms[14] and are a platform for the development of micro- and nanorobots.[15,16] As the length scale of a swimmer decreases, viscous forces acting on it become dominant, and hence inertia no longer plays a role in swimming. This is known as the regime of low Reynolds number. While conventional swimming strategies become ineffective, new propulsion schemes have been devised and experimentally verified,[7,16−19] including the diffusiophoresis of Pt-coated Janus microparticles[3] and the self-electrophoresis of Pt−Au nanorods in aqueous H_2O_2 solutions.[9,20] All these schemes require an anisotropic structure for the motor. However, the smaller the length scale, the more difficult it is to realize the anisotropic structure and the more dominant the randomizing Brownian forces become (the translational diffusion constant of a Brownian particle scales with $1/r$, the rotational diffusion constant with $1/r^3$). Nevertheless, evidence suggesting that an "active" contribution to the motion may even play a role in enzymes, that are reported to show enhanced diffusion when they are catalytically active,[21] has motivated us to try and realize catalytically active nanomotors that are of a comparable size to that of enzymes and to devise a scheme that permits the observation of active motion in the presence of very strong stochastic forces.

Herein, we report the parallel wafer-scale fabrication (>10^{12} particles/hour) of Pt−Au Janus nanoparticles (JNPs) with an overall size of ∼30 nm and demonstrate their catalytic swimming behavior in aqueous solutions of hydrogen peroxide. To the best of our knowledge, the Janus nanoparticles of this Letter are the smallest artificial nanomotors reported to date. The ellipsoidal shape of the JNPs allows us to simultaneously measure both the translational and rotational Brownian motion by dynamic light scattering (DLS). Due to their small size, the Janus nanomotors experience fast rotational Brownian motion which severely limits the ballistic swimming length, nevertheless the JNPs show enhanced diffusion induced by their catalytic activity.

30 nm Pt−Au Janus nanoparticles, as shown in Figure 1, were grown using a physical vapor deposition scheme recently developed by our group.[22] Briefly, a hexagonal array of platinum nanoparticles (NPs) was produced by block copolymer micelle lithography[23] (BCML) on a piranha-cleaned silicon wafer with a particle density of ∼3 × 10^{10} NPs/cm^2

Received: January 7, 2014
Revised: March 25, 2014
Published: April 7, 2014

   dx.doi.org/10.1021/nl500068n | *Nano Lett.* 2014, 14, 2407−2412

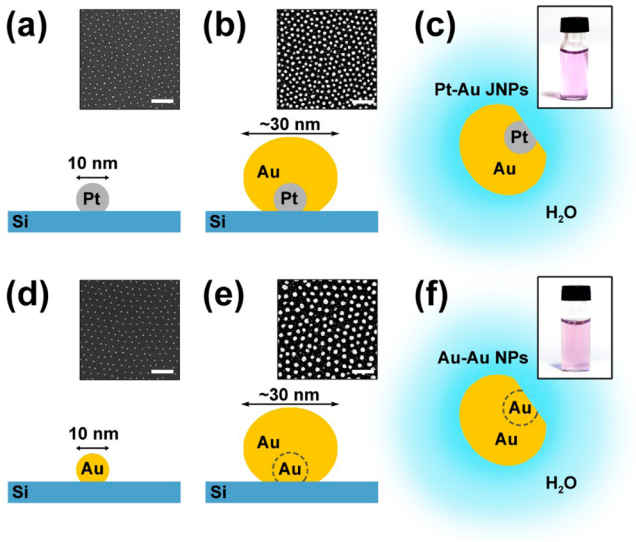

Figure 1. Fabrication scheme of (a)–(c) 30 nm Pt–Au Janus nanoparticles and (d)–(f) Au–Au nanoparticles. (a) A hexagonal array of Pt-nanoseeds was generated by block copolymer micelle lithography on silicon wafer. Inset: Scanning electron micrograph (SEM) of the resultant nanopatterned surface. Scale bar = 200 nm. (b) Elemental gold was deposited onto the Pt-nanoseeds by glancing angle deposition (GLAD) producing an array of Pt–Au Janus nanoparticles. Inset: SEM of the resultant Pt–Au JNPs. Scale bar = 200 nm. (c) Pt–Au JNPs can be lifted off easily by sonication to yield a stable aqueous nanocolloidal solution. Inset: Photograph showing Pt–Au JNPs nanocolloidal solution in a glass vial. (d)–(f) As a control experiment, the same fabrication was repeated on an array of Au-nanoseeds to produce Au–Au nanoparticles.

(Figure 1a). The NP size and the interparticle spacing can be controlled by adjusting the relative amount of Pt-salt and the chain length of the hydrophobic block of the polymer, respectively. Elemental gold was then deposited by glancing angle deposition[24−26] (GLAD) under fast substrate rotation onto the Pt NP-patterned wafer, where each individual Pt NP acted as a nanoseed for the deposition of gold vapor (Figure 1b). The combination of the oblique incident angle of the vapor flux and the fast rotation of the substrate ensures a smooth coverage of the Pt nanoseeds with metallic gold, resulting in a Janus-type Au NP with an embedded Pt NP on one face. The geometry of the resultant JNPs can be controlled by the rotation speed, angle of incidence, and the deposition rate. We have intentionally grown nanomotors that are slightly aspherical, that is ellipsoidal or "oblate spheroidal", such that we can simultaneously measure both the translational and rotational diffusion by DLS (see below). The growth of the Pt–Au Janus nanoparticles typically requires less than 1 h, and each deposition run can generate $\sim 10^{12}$ JNPs on a 3-in. wafer. This generic fabrication scheme also allows us to grow JNPs of other materials, such as Pt–Mg and Pt–Fe, for potential biological applications.[27] After the fabrication step, the JNPs can be easily detached from the wafer by sonicating a piece of the wafer in an aqueous solution of 1 mM sodium citrate, which produces a stable nanocolloidal solution. A piece of 1 cm^2 sample wafer yields $\sim 3\times 10^{10}$ NPs in a 1 mL solution which is about the same concentration as that of commercial Au NP solutions for this size.[28] The asymmetric Pt inclusion of the JNP has one face exposed to the solution (Figure 1c) and can thus catalyze the disproportionation of hydrogen peroxide. As a control experiment, we have also repeated the fabrication on a wafer patterned with Au-nanoseeds to generate nanocolloidal solutions of Au–Au nanoparticles (Figure 1d–f).

The shape of the resultant Pt–Au JNPs was characterized by transmission electron microscopy (TEM, see Figure 2a). The

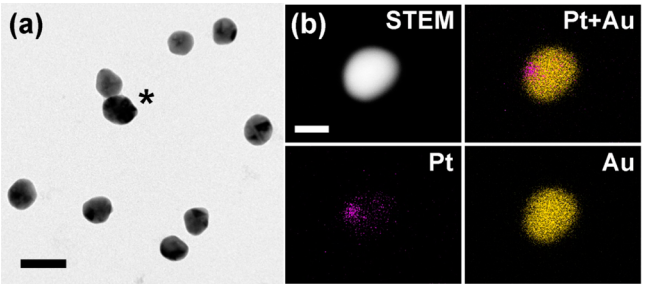

Figure 2. (a) Transmission electron micrograph of 30 nm Pt–Au JNPs. Dimers (marked by an asterisk) are observed to be ~5% of the entire population. (b) High-angle annular dark field (HAADF) STEM image and STEM-edx elemental maps of a selected Pt–Au JNP. Scale bars: (a) 50 nm; (b) 20 nm.

designed ellipsoidal geometry of the JNPs was confirmed with $2a = 33.3 \pm 3.6$ nm, $2b = 28.8 \pm 3.2$ nm, and an eccentricity $\varepsilon = 0.45 \pm 0.18$, based on a statistical analysis of over 200 particles. The as-fabricated JNPs exist mostly as individual monomers, while dimers and oligomers are observed to be ~5% of the whole population. These dimers and oligomers were probably formed during the deposition process from adjacent Pt-nanoseeds that are too close to each other and are hence joined by the deposited gold. The low abundance of dimers in the samples, as well as the overall sample monodispersity and purity, are critical to DLS measurements. The samples produced by our fabrication scheme fulfill the above requirements as shown by the TEM and DLS data (see below). In order to confirm the material composition of the 30 nm Pt–Au JNPs, elemental distribution maps were obtained by scanning transmission electron microscopy-energy dispersive X-ray (STEM-edx) spectroscopic imaging on a single JNP as shown in Figure 2b. As expected, the elemental maps show the asymmetrically embedded 10 nm platinum nanoparticle. The Pt NP is displaced off-center on the minor axis, leading to a $C_{\infty v}$ point group symmetry (in Schönflies notation) for the JNP.

As a control, we have also fabricated 60 nm Pt–Pt–Au JNPs by a similar scheme (see SI Figure S1). Unlike the 30 nm JNPs, the slightly larger size of the 60 nm JNPs allows for direct single particle tracking with dark field optical microscopy. Figure 3a shows selected trajectories of 60 nm Pt–Pt–Au JNPs in water both with and without H_2O_2 (see the SI for movies). It is challenging to resolve the motion of such small JNPs in water due to their fast 3-D Brownian motion and the low intensity of the scattered light. Hence, we increased the viscosity to slow the JNPs down by using a 50% water-glycerol mixture. This effectively increases the dynamic viscosity ~8 fold with respect to that of pure water, therefore permitting the use of a longer integration time *per* video frame. Mean squared displacements (MSD) of the 60 nm JNPs are plotted against time in Figure 3b. From the slope of the plot, translational diffusion constants D can be extracted, with $D = \mathrm{MSD}/4t$, giving $D = 1.0 \pm 0.3$ $\mu m^2/s$ in the absence of H_2O_2. This value agrees with the theoretical Brownian diffusion constant (= 1.06 $\mu m^2/s$) given by Stokes' Law. In the presence of 1.5% H_2O_2, the apparent diffusion of the JNPs increases by ~50% to 1.5 ± 0.8 $\mu m^2/s$. The results from the dark field optical microscopy tracking

dx.doi.org/10.1021/nl500068n | Nano Lett. 2014, 14, 2407−2412

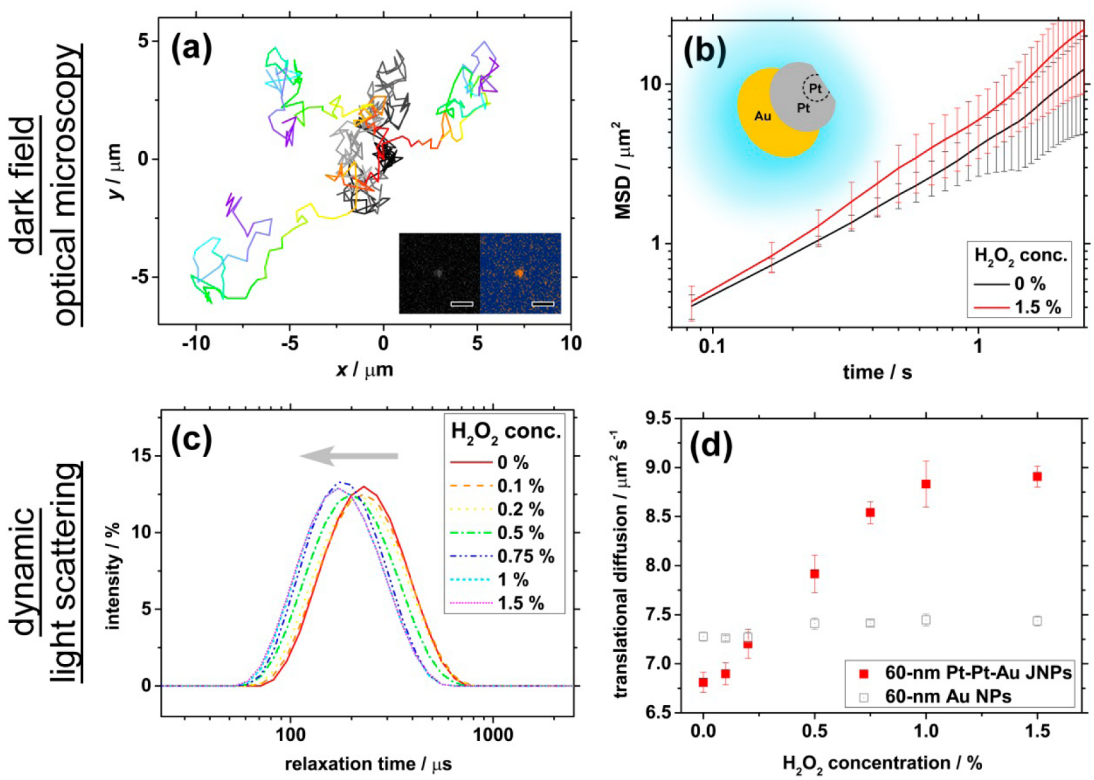

Figure 3. Enhanced diffusion of 60 nm Pt−Pt−Au JNPs in various H_2O_2 concentrations as observed by (a)−(b) single particle tracking using dark field optical microscopy and (c)−(d) dynamic light scattering measurements. (a) Selected trajectories of Pt−Pt−Au JNPs in 0% (gray scale tracks) and 1.5% H_2O_2 (colored scale tracks); 3, 6-s centered tracks for each. The measurements were carried out in 50% aqueous glycerol. Inset: dark field optical microscopy image of a single 60 nm Pt−Pt−Au JNP (left) and the same image plotted in false color scale (right); scale bars = 2 μm. (b) Mean squared displacements (MSD) of Pt−Pt−Au JNPs plotted against time. Inset: schematic diagram of a Pt−Pt−Au JNP. (c) Translational relaxation time of 60 nm Pt−Pt−Au JNPs for different H_2O_2 concentrations measured by dynamic light scattering. Gray arrow indicates the systematic decrease in relaxation time with increasing H_2O_2 concentration. (d) Translational diffusion constants of 60 nm Pt−Pt−Au JNPs plotted against H_2O_2 concentration. Data of 60 nm commercial Au NPs was shown for comparison.

experiments were compared with DLS measurements (Figure 3c, d). The larger sampling size of DLS enables measurements with a higher time resolution (μs), hence allowing the use of water as dispersant. The Brownian diffusion constant of 60 nm JNPs as measured by DLS is 6.8 ± 0.1 $\mu m^2/s$ which is slightly smaller than that determined by dark field microscopy, where the corresponding diffusion constant corrected for differences in the dynamic viscosity is found to be 7.6 $\mu m^2/s$. The observed difference is consistent with the fact that DLS measures the hydrodynamic size of a particle which is always larger (i.e., smaller D) than the actual size of the particles. In agreement with the results from dark field microscopy, the apparent diffusion constant, as measured by DLS, increases with H_2O_2 concentration.

Dark field microscopy and DLS could both verify the enhanced diffusion of the 60 nm JNPs, but for the smaller 30 nm JNPs we focus on DLS measurements, as dark field optical microscopy is not sensitive enough to reliably monitor the motion of such small nanomotors. An advantage of the DLS measurements is that the rotational diffusion relaxation time can be directly approximated for the ellipsoidal Pt−Au JNPs (Figure 4a), see SI Section S3 for a detailed discussion.[29,30,31] Particle shape anisotropy allows for the distinction of rotational diffusion due to intensity fluctuations arising from particle tumbling; however, particles which are spherical can also give rise to intensity fluctuations if they are optically anisotropic.[32] The rotational relaxation time plays an important role in determining the persistence of the nanomotors. The observed rotational diffusion relaxation times of Pt−Au JNPs and Au−Au NPs in 1 mM sodium citrate solution are 11.6 ± 0.7 μs and 12.2 ± 0.8 μs, respectively. These values correspond closely to the theoretical rotational relaxation time of 12.7 μs for a 50 nm sphere in water based on Stokes equation for rotational Brownian motion. The translational diffusion constants of the Pt−Au JNPs and Au−Au NPs are 10.2 ± 0.1 $\mu m^2/s$ and 10.4 ± 0.2 $\mu m^2/s$, corresponding to a hydrodynamic diameter of 53.4 and 52.5 nm, respectively. The somewhat larger-than-expected hydrodynamic diameters are probably due to the contribution of a few dimers and oligomers in the samples. Although only present in a small proportion, these oligomers will contribute more to the scattering signals, which scale with r^6, where r is the radius of the scatterer. The scattering contribution from a small number of larger particles can be filtered by analyzing the data based on the volume distribution, which gives a hydrodynamic diameter of 29.7 and 34.6 nm for the Pt−Au JNPs and Au−Au NPs, respectively. These radii match well with the TEM analysis. However, data based on scattering volume is more susceptible to measurement errors (see SI section S4), and, therefore, the subsequent DLS analysis is solely based on scattering intensity data.

Upon addition of hydrogen peroxide to a nanocolloidal solution of 30 nm Pt−Au JNPs, disproportionation of H_2O_2 is catalyzed by the Pt−Au metal couple, where oxygen molecules will be generated at the Pt anode.[20] During this process,

dx.doi.org/10.1021/nl500068n | Nano Lett. 2014, 14, 2407−2412

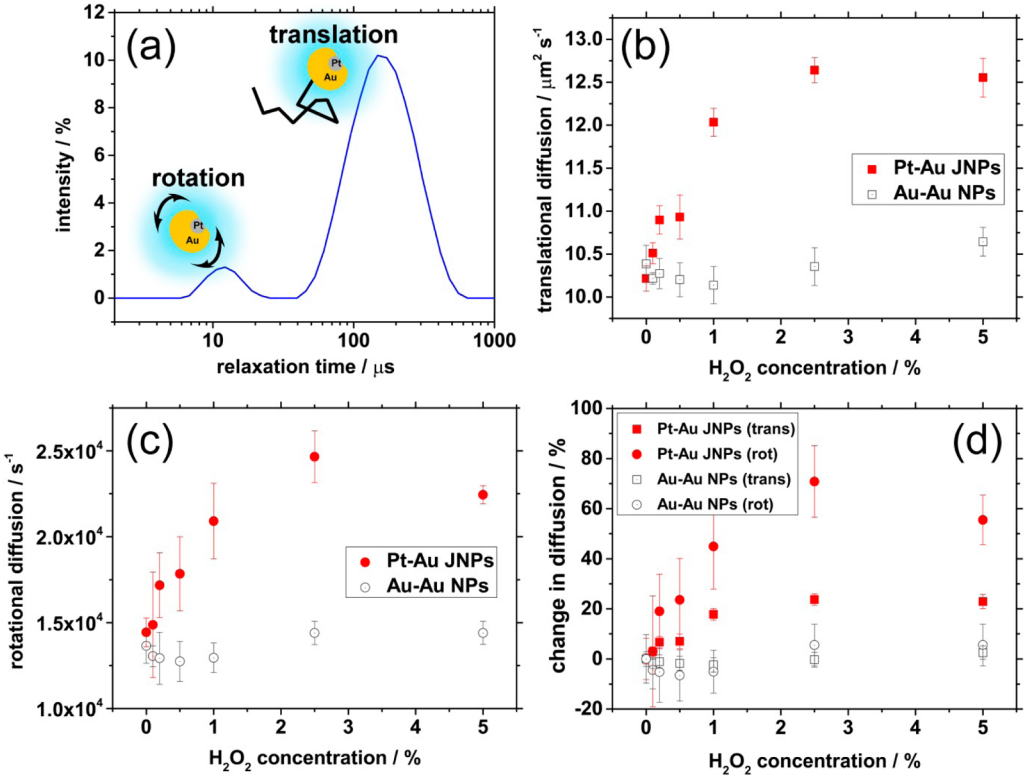

Figure 4. (a) Translational and rotational relaxation plot of the 30 nm Pt−Au JNPs in 1 mM sodium citrate solution as measured by dynamic light scattering. Averages of spectra (based on at least 5 measurements) are used for subsequent analysis (see SI Section S3 for details). Apparent (b) translational and (c) rotational diffusion constants of Pt−Au JNPs and Au−Au NPs for different concentrations of H_2O_2. Each data point represents a weighted average ($= \Sigma x_i y_i / \Sigma y_i$) of the corresponding relaxation peak. (d) Percentage change of translational and rotational diffusion constants as a function of the H_2O_2 concentration.

electrons flow from the Pt anode to the Au cathode, and this electric charge imbalance will be neutralized by the flow of ions along the JNP's surface which results in the nanomotor's propulsion in the opposite direction, i.e. here toward the Pt end (Figure 5a). This mechanism is known as self-electrophoresis.[9,20] We find that the Pt−Au JNPs show a significant increase in both translational and rotational diffusion constants with increasing concentration of H_2O_2 (Figure 4b−d). This increase appears to be linear with the H_2O_2 concentration before it saturates at ∼2.0% (v/v) H_2O_2. For the control Au−Au NP sample, no significant increase in diffusion was observed with increasing H_2O_2 concentration, as is expected. The slight initial decrease in diffusion is consistent with the small increase in dynamic viscosity of the solvent mixture upon addition of H_2O_2. The control experiments verify that the Pt−Au JNPs show an increase in their diffusion with increasing H_2O_2 concentrations, and this increase in diffusion is attributed to the catalytically active Pt. At a very high H_2O_2 concentration the formation of macroscopic gas bubbles was observed in the Pt−Au JNP solutions but not for the Au−Au NP solutions, which confirms that the embedded Pt in the JNP is catalytically active (see SI section S5). Nevertheless, the presence of catalytically active Pt alone is not sufficient for the propulsion of nanomotors. Unlike irregularly shaped Pt microparticles which can self-propel by random fluctuation of surface reaction rate,[33] nanoparticles of 30 nm in size are highly symmetric and therefore cannot maintain an appreciable concentration gradient across the particle (via random fluctuations). Hence, the asymmetric Janus nanostructure serves as another necessary criterion for the propulsion of nanomotors, as the resultant anisotropy of the chemical reaction allows propulsion via self-phoresis. This is verified by a control experiment using commercial 30 nm Pt NPs and 30 nm Pt−Pt NPs made by our GLAD system, where the presence of H_2O_2 was found to have a negligible effect on the diffusion constant, despite the observation of gas bubbles (see SI section S6). Finally, to further rule out the unlikely possibility that the propulsion of the JNPs is caused by nanoscale bubbles formed in solution, we have mixed in a small amount of inactive polystyrene particles to a nanocolloidal solution of 30 nm Pt−Au JNPs in the presence of H_2O_2 (see SI section S7). The absence of enhanced diffusion of the inactive polystyrene particles provides further evidence that the active motion of the JNP nanomotors is caused by local electrophoretic effects across the JNPs, rather than the perturbation due to gas bubbles formed in the solution (if they exist at all).

We deduce an average ballistic swimming length and the average speed of the Pt−Au JNPs from the relation: $D_{app} = D_0 + l^2/4\tau$, where D_{app} is the apparent translational diffusion constant for a particular H_2O_2 concentration, D_0 is the translational diffusion constant in the absence of H_2O_2, l is the average ballistic persistence length, and τ is the rotational relaxation time.[3] The average speed, v, of the nanomotor follows from the average linear displacement for a time interval between rotations, τ. The effect of the H_2O_2 concentration on τ, l, and v are shown in Figure 5. Although the rotational relaxation decreases with increasing H_2O_2 concentration, the average persistence length is found to increase with the H_2O_2 concentration. It suggests that the JNPs move at a greater average speed in-between each rotation. The average ballistic

dx.doi.org/10.1021/nl500068n | Nano Lett. 2014, 14, 2407−2412

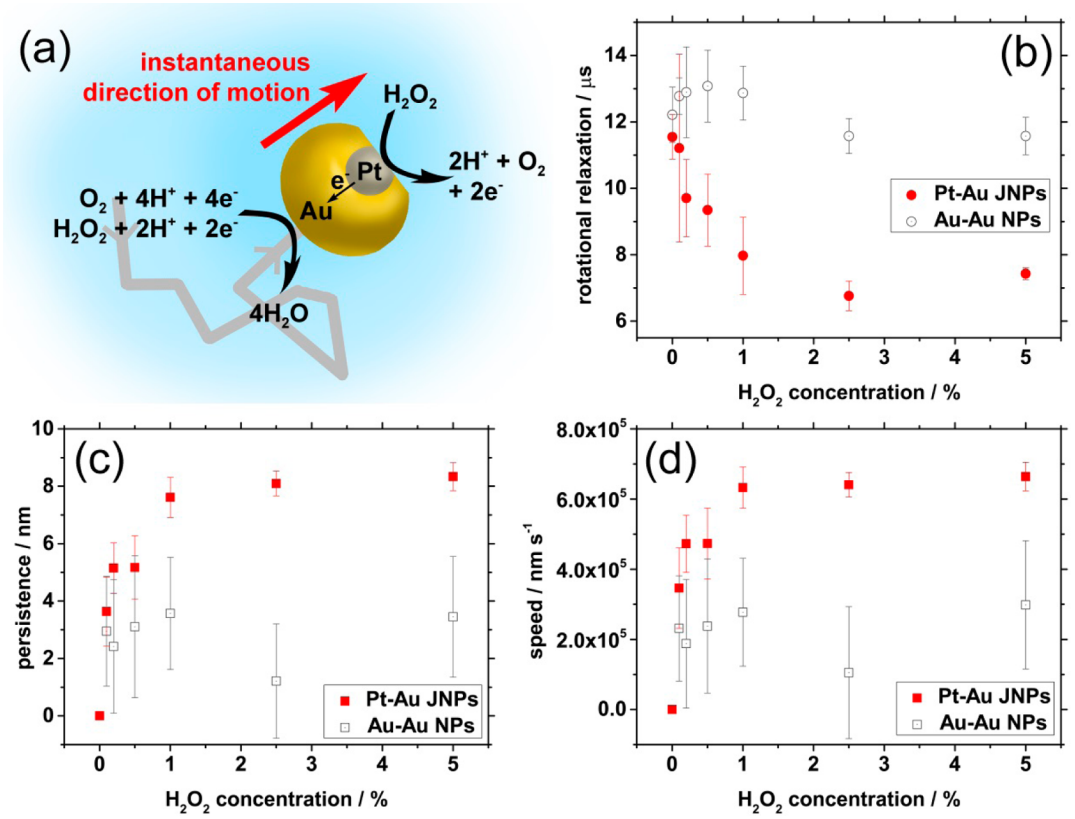

Figure 5. (a) Self-electrophoresis of a Pt–Au JNP via catalytic disproportionation of H_2O_2. A gradient of electric charge density will be generated across the JNP as reaction proceeds. Electro-osmotic flow induced by the charge imbalance will then cause the JNP to move in a direction opposite to that of the fluid flow (red arrow), as described in previous reports.[20] (b) Apparent rotational relaxation times τ, (c) average ballistic swimming length/persistence l, (d) average speed v of the 30 nm Pt–Au JNPs and Au–Au NPs in various concentration of H_2O_2. l and v are calculated based on equations $D_{app} = D_0 + l^2/4\tau$ and $v = l/\tau$. For Au–Au NPs, since D_{app} is not always greater than D_0, absolute values of their difference are taken when calculating l to ensure it is a real number. Theoretical value (= 0) of persistence and speed at 0% H_2O_2 are included in the corresponding plots.

swimming speed increases linearly with H_2O_2 concentration up to a value of 0.66 ± 0.04 mm/s (~2.2×10^4 body lengths/s) at a H_2O_2 concentration of ~1.5% with a corresponding Reynolds number of ~2×10^{-5}. These are very fast bursts in-between rotations. However, because of the small size, the rotational diffusion dominates and the JNPs rapidly reorient which results in enhanced diffusion induced by the catalytic self-electrophoresis.

In conclusion, we have demonstrated the wafer-scale fabrication of Pt–Au Janus nanoparticles with high yield, monodispersity, and fidelity in the structure and material composition. The designed shape and optical anisotropy of the JNPs allows their translational and rotational Brownian motion to be directly observed with dynamic light scattering. Given an overall size of ~30 nm, the characteristic length of the Pt–Au Janus nanoparticles approaches the size of larger enzymes. It has recently been proposed that enhanced diffusion can be observed in chemically active enzymes and that this may be caused by the nonreciprocal conformational change during the catalytic cycle of the enzymes.[21,34−36] The artificial JNPs of this Letter indeed show enhanced diffusion when they are catalytically active but do so via self-electrophoresis. The small size of the nanomotors suggests that the conventional phoretic swimming mechanisms, e.g. self-electrophoresis[20] or self-diffusiophoresis,[37] can also be effective at the nanoscale, and this may play a role in molecular systems. While having a ballistic speed of ~2.2×10^4 body lengths/s in 1.5% H_2O_2, the fast rotational Brownian motion poses an upper limit on the ballistic swimming length of the nanomotors. For longer-range ballistic motion at the nanoscale, it is necessary to reduce the Brownian rotation rate, which could for instance be achieved near a surface and under geometric confinement, for example by a nanofiber or within a nanochannel. In contrast, another possible (and perhaps wise) approach for designing nanomotors and active nanosystems is to utilize the inherent Brownian motion rather than work against it. As shown in a simulation study on substrate-enhanced diffusion of enzymes,[21] the artificial nanomotors of this Letter are also expected to have chemotactic behavior toward the chemical fuel as a result of substrate-enhanced diffusion. It is interesting to ask whether the active motion of nanoscale Janus-like catalysts can induce higher turnover *per* active surface area compared with regular catalysts in reactions that are diffusion limited. Furthermore, our artificial nanomotors can have implications on size-effects in nanofluidics and serve as model systems to explore hydrodynamic effects in the size-regime of macromolecules, molecular nanomotors, and at the limit of continuum hydrodynamics.

■ ASSOCIATED CONTENT

Supporting Information

Experimental procedures, additional DLS data and TEM images, apparent hydrodynamic size, control experiments using 30 nm Pt NPs, and dark field optical microscopy movies. This material is available free of charge via the Internet at http://pubs.acs.org.

dx.doi.org/10.1021/nl500068n | *Nano Lett.* 2014, 14, 2407−2412

AUTHOR INFORMATION

Corresponding Author

*E-mail: fischer@is.mpg.de.

Author Contributions

T.-C.L. initiated this project. C.M. prepared nanopatterns and grew the NPs. M.A.-C. prepared the nanocolloidal solutions and conducted bright field TEM imaging and dynamic light scattering measurements. T.-C.L. characterized the JNPs by HAADF-STEM and STEM-edx, and K.H. assisted. J.G.G. carried out particle tracking by dark field optical microscopy. T.-C.L., M.A.-C., J.G.G., and P.F. analyzed the data and wrote the paper.

Notes

The authors declare no competing financial interest.

ACKNOWLEDGMENTS

The authors are grateful to J. P. Spatz for providing SEM access and support with the micelle nanolithography. We are grateful to F. Höfling, H.-H. Jeong, and T. Qiu for helpful comments. This work was in part supported by the European Research Council under the ERC Grant agreement 278213.

REFERENCES

(1) Ebbens, S. J.; Howse, J. R. *Soft Matter* **2010**, *6*, 726.
(2) He, Y.; Wu, J.; Zhao, Y. *Nano Lett.* **2007**, *7*, 1369.
(3) Howse, J. R.; Jones, R. A. L.; Ryan, A. J.; Gough, T.; Vafabakhsh, R.; Golestanian, R. *Phys. Rev. Lett.* **2007**, *99*, 048102.
(4) Ke, H.; Ye, S.; Carroll, R. L.; Showalter, K. *J. Phys. Chem. A* **2010**, *114*, 5462.
(5) Laocharoensuk, R.; Burdick, J.; Wang, J. *ACS Nano* **2008**, *2*, 1069.
(6) Liu, R.; Sen, A. *J. Am. Chem. Soc.* **2011**, *133*, 20064.
(7) Mei, Y.; Solovev, A. A.; Sanchez, S.; Schmidt, O. G. *Chem. Soc. Rev.* **2011**, *40*, 2109.
(8) Palacci, J.; Sacanna, S.; Steinberg, A. P.; Pine, D. J.; Chaikin, P. M. *Science* **2013**, *339*, 936.
(9) Paxton, W. F.; Kistler, K. C.; Olmeda, C. C.; Sen, A.; St. Angelo, S. K.; Cao, Y.; Mallouk, T. E.; Lammert, P. E.; Crespi, V. H. *J. Am. Chem. Soc.* **2004**, *126*, 13424.
(10) Poon, W. *arXiv preprint arXiv:1306.4799* 2013.
(11) Qin, L.; Banholzer, M. J.; Xu, X.; Huang, L.; Mirkin, C. A. *J. Am. Chem. Soc.* **2007**, *129*, 14870.
(12) Wheat, P. M.; Marine, N. A.; Moran, J. L.; Posner, J. D. *Langmuir* **2010**, *26*, 13052.
(13) Wilson, D. A.; Nolte, R. J.; van Hest, J. C. *Nat. Chem.* **2012**, *4*, 268.
(14) Jülicher, F.; Ajdari, A.; Prost, J. *Rev. Mod. Phys.* **1997**, *69*, 1269.
(15) Mallouk, T.; Sen, A. *Sci. Am.* **2009**, *300*, 72.
(16) Wang, J. *Nanomachines*; John Wiley & Sons: 2013.
(17) Dreyfus, R.; Baudry, J.; Roper, M. L.; Fermigier, M.; Stone, H. A.; Bibette, J. *Nature* **2005**, *437*, 862.
(18) Ghosh, A.; Fischer, P. *Nano Lett.* **2009**, *9*, 2243.
(19) Jiang, H.-R.; Yoshinaga, N.; Sano, M. *Phys. Rev. Lett.* **2010**, *105*, 268302.
(20) Wang, Y.; Hernandez, R. M.; Bartlett, D. J.; Bingham, J. M.; Kline, T. R.; Sen, A.; Mallouk, T. E. *Langmuir* **2006**, *22*, 10451.
(21) Sengupta, S.; Dey, K. K.; Muddana, H. S.; Tabouillot, T.; Ibele, M. E.; Butler, P. J.; Sen, A. *J. Am. Chem. Soc.* **2013**, *135*, 1406.
(22) Mark, A. G.; Gibbs, J. G.; Lee, T.-C.; Fischer, P. *Nat. Mater.* **2013**, *12*, 802.
(23) Glass, R.; Möller, M.; Spatz, J. P. *Nanotechnology* **2003**, *14*, 1153.
(24) Hawkeye, M. M.; Brett, M. J. *J. Vac. Sci. Technol., A* **2007**, *25*, 1317.
(25) Robbie, K.; Brett, M. *J. Vac. Sci. Technol., A* **1997**, *15*, 1460.
(26) Zhao, Y.-P.; Ye, D.-X.; Wang, G.-C.; Lu, T.-M. *Nano Lett.* **2002**, *2*, 351.
(27) Mou, F.; Chen, C.; Ma, H.; Yin, Y.; Wu, Q.; Guan, J. *Angew. Chem.* **2013**, *125*, 7349.
(28) Sigma Aldrich #741981.
(29) Berne, B. J.; Pecora, R. *Dynamic light scattering: with applications to chemistry, biology, and physics*; Courier Dover Publications: New York, 2000.
(30) Glidden, M.; Muschol, M. *J. Phys. Chem. C* **2012**, *116*, 8128.
(31) Günther, A.; Bender, P.; Tschöpe, A.; Birringer, R. *J. Phys.: Condens. Matter* **2011**, *23*, 325103.
(32) Lehmuskero, A.; Ogier, R.; Gschneidtner, T.; Johansson, P.; Käll, M. *Nano Lett.* **2013**, *13*, 3129.
(33) Yamamoto, D.; Mukai, A.; Okita, N.; Yoshikawa, K.; Shioi, A. *J. Chem. Phys.* **2013**, *139*, 034705.
(34) Cressman, A.; Togashi, Y.; Mikhailov, A. S.; Kapral, R. *Phys. Rev. E* **2008**, *77*, 050901.
(35) Golestanian, R. *Phys. Rev. Lett.* **2010**, *105*, 018103.
(36) Sakaue, T.; Kapral, R.; Mikhailov, A. *Eur. Phys. J. B* **2010**, *75*, 381.
(37) Golestanian, R.; Liverpool, T. B.; Ajdari, A. *Phys. Rev. Lett.* **2005**, *94*, 220801.